Fault Classification and Diagnosis of UAV motor Based on Estimated Nonlinear Parameter of Steady-State Model

Jun-yong Lee, Won-tak Lee, Sang-ho Ko, and Hwa-suk Oh
Korea Aerospace University, Goyang, South Korea
Email: {supermundane@naver.com, dnjsxkr526@kau.kr}, {sanghoko, hsoh}@kau.ac.kr

***Abstract*—UAVs are now applied to various fields, from military missions to civilian applications. A malfunction in the drone's thrust system during flights can result in collisions and damages of property or human injury. To prevent this, the tolerant control of the multicopter has been studied to stabilize attitude, but it tends to focus on short-sighted management. In this paper, we propose an overall fault diagnostic technique for the UAV motor itself. To do this, we derive a model for the UAV motor in the normal steady-state using a nonlinear equation, which is then experimentally verified with 99% accuracy. We consider bearing friction increase, phase open, propeller broken, transistor open, and back EMF signal errors for malfunction of UAV motor, and we suggest a simple fault diagnosis algorithm by an analysis of the fault characteristics. We show the effectiveness of our diagnostic technique by the experimental results of the testbed and flight model.**

***Index Terms*—fault diagnosis, hardware-based simulation, modeling, multicopter, nonlinear equations, steady-state, UAV motor**

I. INTRODUCTION

Unmanned aerial vehicles (UAVs) or drones, were originally developed for military purposes, but these days they offer many civil applications such as rescue, delivery, leisure, etc [1]. Especially large shipping companies such as Amazon, DHL, and Google aim to provide delivery services by drones. The drone related accidents have been increased with its number [2]. So far, human factors have been the most common cause of accidents in drone flights [3], [4]. As automation technology advances, human errors will be reduced, but problems related to unscheduled component failure or maintenance will be on the rise. Some defect in the thrust system of a UAV can cause to fail the flights, thus it can be a threat to objects or people. In propulsion systems of UAVs, BLDC type electric motors are commonly applied since they have less vibration and weight than gas engines [5].

The multicopter, which consists of several UAV motors (module with integrated propeller and BLDC motor), has attracted a lot of attention because it is easy to control the attitude and it is possible to operate even if one of the motor has failed [6]. Early researches dealt with detecting or estimating techniques for motor failure by monitoring the performance during attitude control of drones [7]-[10]. Fault isolation [11] and fault tolerant control [12]-[14] techniques were studied because the studies on fault diagnosis focused mainly on overcoming faults with attitude stabilization. Fault tolerant control is only a short-term solution, so long-term solutions such as life prediction of battery, structure fatigue management or UAV motor fault diagnoses should be studied for prevention of failures. For this reason, there has been growing interest in diagnosing the faults of the UAV motor itself. F. Pourpanah developed a monitoring system to detect possible faults of UAV motors and propellers in an early state [15]. A. Bondyra proposed algorithms to detect the occurrence of rotor fault and to determine its scale and type from signal processing to machine learning [16]. A. Benini presented an actuator fault detection algorithm for UAVs, based on time and frequency-domain analysis of acceleration signals and features selection techniques [17]. J. Fu showed a deep-learning-based method to accurately locate actuator faults by using flight data of a real UAV [18]. G. Iannace built a model using an artificial neural network algorithm and tested unbalanced blade detection of the UAV propeller with noise measurements [19]. Most studies about UAV motor faults focused on the rotor integrated with the propeller and did not include any analysis of the overall faults of the motor. On the other hand, studies on fault diagnosis of general BLDC motors have been variously conducted in the last few decades. In [20], and [21], the causes of motor faults are classified as the bearing, stator, rotor, and others. The following studies of fault diagnostics all used this classification. O. Moseler suggested an estimation technique of electrical and mechanical parameters for fault detection on the BLDC type of motors [22]. M. A. Awadallah designed two adaptive neuro–fuzzy inference systems (ANFIS) for fault diagnosis and location of stator-winding interturns in BLDC motors [23], [24]. He developed an intelligent agent based on ANFIS to automate the fault identification and location process, and studied a faulty performance of motor drives under open-switch conditions [25]. S. Rajagopalan proposed two novel methods using windowed Fourier ridges and Wigner–Ville-based

Manuscript received June 14, 2020; revised December 7, 2020.

doi: 10.18178/ijmerr.10.1.22-31

distributions for the detection of rotor faults in brushless DC motors operating under continuous nonstationarity [26]. B. Park presented a simple fault diagnosis scheme for open-circuit fault of motor drives using the measured phase current information [27]. A. Tashakori proposed a fault diagnostic technique that can identify fault type and the faulty switch to an inverter based on the discrete fourier transform (DFT) analysis of the measured line voltages of 3-phase drives of a BLDC motor [28]. J. Fang suggested an online model-based inverter fault diagnosis method, which can detect and identify both open-circuit and short-circuit damages of a single switch for buck converters or 3-phase full bridge inverters of BLDC motors [29]. Compared to general DC motors, A UAV motor that is affected by the propeller may have a different model and causes of faults. Since a precisly estimated model is similar to the real state, it can predict the output accurately and it has the advantage in fault diagnosis.

This paper proposes a suitable model and a fault-diagnosis technique using the steady state conditions for a UAV motor. By the steady state assumption, DC motor models can be simplified because derivative terms are removed. As a result, the parameters of the models are estimated more accurately and stably for steady state than in the transient state. Compared to the general motor model, the proposed model is nonlinearly related to angular speed and depends on the friction torque caused by thrust. This paper deals with overall faults that can occur to the UAV motors and suggests a detailed method to simulate the faults. The faults are classified as bearing, stator, rotor, and others and are analyzed based on steady state. We design a diagnostic algorithm for UAV motor faults to distinguish each fault including normal operation. The experimental results of a testbed verify the suitability of the proposed UAV motor model and show the effectiveness of the diagnostic algorithm. Moreover, hovering experiments of the hexacopter shows that the fault diagnosis is applicable even for the flight models.

II. UAV Motor Modelling

In this section, a mathematical process model will be derived for UAV motors. First, the steady state model of general DC motors is summarized. The equivalent circuit of a DC motor is simplified based on the fact that the coil winding has a resistance R, a self-inductance L and an induced back EMF [30]. Voltage equation of DC motors is given by

$$V = L\frac{di}{dt} + Ri + k_e \omega \tag{1}$$

where k_e and ω denote back-EMF constant and rotation speed of the motor respectively. For steady state, the coil current is constant and hence the rate of change of the coil current is zero. Hence the voltage equation reduces to

$$V = Ri + k_e \omega \tag{2}$$

A generic mechanical equation of the DC motors consists of inertial torque, friction, and load torque. It is given symbolically as

$$T_g = J\frac{d\omega}{dt} + B\omega + T_f + T_l \tag{3}$$

where J is a moment of inertia of the rotor which includes the assembled structure, B is a damping coefficient associated with the rotational system of the machine, T_f is the static or dynamic friction torque, T_l is the load torque, and T_g is the electromagnetic torque. In the case of a motor, the input is electrical energy and the output is the mechanical energy. So the generated torque by electromagnetic force determines the acceleration, speed, and position of the rotor and it is proportional to the coil current [31]. In the steady state, angular acceleration converges to zero if there is no external torque. The mechanical equation of the motors can be derived as follows

$$k_t i = B\omega + T_f \tag{4}$$

where k_t is the torque constant which has the same quantity to back-EMF constant.

A. Nonlinear Modelling for UAV motor

A UAV motor is equipped with a propeller on a BLDC motor to generate thrust. When the propeller rotates, thrust in the direction of the rotation axis is generated aerodynamically. As thrust is transmitted from the propellers to the vehicle, additional friction is generated in the motor by normal forces act on the bearings. Considering this additional friction in mechanical equations of the DC motors, this paper proposes an adaptive model for UAV motors. Many studies have verified a relationship between thrust and speed of a propeller in both theory and experimental results [32], [33]. The mathematical model of thrust can be calculated by

$$F_T = C_T \rho D^4 \omega^2 \tag{5}$$

where C_T is thrust coefficient, ρ is air density, D is the diameter of the propeller, and F_T is the thrust. If a UAV motor is fixed, thrust coefficient and diameter of the propeller are constants. In most of the available models, air density is considered constant too. There are modelling studies in which the relationship between friction torque and thrust is assumed to be linear [34], [35]. But such models have only been theoretically simulated, and moreover they were not able to be verified experimentally. It has been experimentally proved that the mechanical model of bearings is complicated and depends on bearing types, the contact angle of balls, the materials and et al [36], [37]. One study has suggested the propeller model as a power function of speed, and furthermore experimental results have shown that the modelling is fairly accurate [38]. The equation of friction torque by a propeller can be expressed by

$$T_p = C_p \omega^k \tag{6}$$

where T_p is a generated friction torque by propeller, k is an exponent of angular speed, and C_p can be defined as a proportional factor by the aerodynamic properties. Joining (4) with (6), a mechanical model of UAV motors can be derived as

$$k_t i = C_p \omega^k + B\omega + T_f \tag{7}$$

As a result, we suggest (7) as the model of UAV motors, which is a nonlinear equation for the steady state.

B. Estimation of the Model Parameters of UAV Motor

We made the testbed which consists of a UAV motor and electronic speed control (ESC) to experiment on the ground. The UAV motor includes a BLDC motor (sunnysky X2212) and a propeller (DJI Phantom 3-9450), and ESC (ZTW spider oneshot125) can control the input voltage to pulse width modulation (PWM). In general, low and middle cost UAVs use products of a similar type to have given hardware models. If a UAV requires a different range of angular speed or torque, then the hardware can be changed. Table 1 shows the specifications of the UAV motor which is used in the testbed.

In this paper, the phase resistance and the motor constant were estimated for verification, although these are given as a specification. A test for an estimation of parameters was set to 11 equivalent points for the voltage range that is 4 to 11 V. Measurements of angular velocity and current are obtained during a steady state for 5 minutes at each voltage point. As Fig. 1 clearly shows the nonlinearity of velocity-current, the proposed model confirmed the applicability. Levenberg-Marquardt (LM) method for nonlinear least squares estimation is used to solve (2) and (7). The standard method consists of minimizing the given equations:

$$S = \sum_{j=1}^{n} ({y_t}^j - {y_m}^j)^2 \tag{8}$$

where n is the number of data sets, y_m is a measurement and y_t is a theoretical value which is calculated by the model. As a first step, the phase resistance and the motor constant are estimated by voltage equations. Theoretical voltage is calculated from the measurement of current and angular velocity, which can be represented by the following equation:

$$V_t = R i_m + k_e \omega_m \tag{9}$$

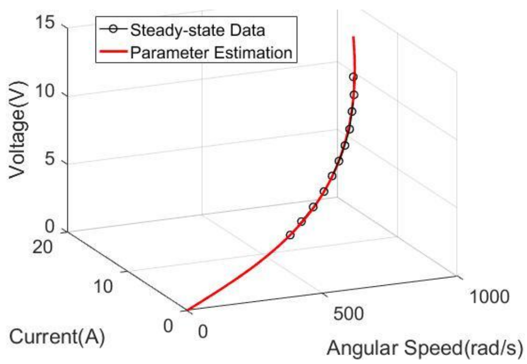

Figure 1. A comparison of the steady-state input voltage between the average measurements and estimated value from (9).

TABLE I. SPECIFICATION AND PARAMETERS OF THE UAV MOTOR

Items	Values	Units
DC motor dimension	Ø27.5/H42.0	[mm]
DC motor weight	56	[g]
Phase resistance	160	[mΩ]
Bus voltage	11.1	[V]
Motor constant	9.74	[mNm/A]
Maximum power	300	[W]
Propeller dimension	240	[mm]
Propeller weight	24	[g]

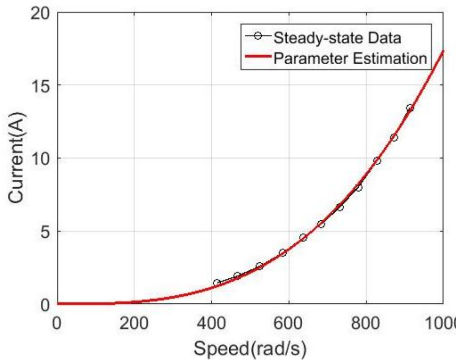

Figure 2. A comparison of the steady-state output current between the average measurements and estimated value from (10).

The estimation result shows that a phase resistance of 0.165 Ω and a motor constant of 9.75 mNm/A. The error of the parameters was respectively 3.1% and 0.1%, hence it was verified that it was similar to the specifications of the UAV motor. A 3-dimensional plot of the steady state data in comparison with the estimated voltage equation is shown in Fig. 1. In the second step, parameters of the mechanical equation are estimated by the equations:

$$i_t = \frac{C_p}{k_t} {\omega_m}^k + \frac{B}{k_t} \omega_m + \frac{T_f}{k_t} \tag{10}$$

where k_t is the estimated motor constant, i_t is a theoretical current which is calculated from the measurement of angular velocity. In addition, k is considered a positive integer because of simplicity when equations of angular speed and current are converted to function of voltage. This assumption was required because a processor predicts the output of current and speed of the voltage input when the state of the UAV motor is analyzed. Similar to the voltage equation, parameters of (10) estimate to use the nonlinear least squares by comparing theoretical current with measurement. The proportional factor C_p, the damping coefficient and the dynamic friction torque are estimated 1.692E-10 $\mathrm{Nm/(rad/s)^3}$, 1.275E-7 Nm/(rad/s) and 4.606E-10 Nm respectively. The exponent k is estimated to be 3 which is closest to the positive integer. Estimated mechanical modeling of the UAV motor is compared with the measured values in the angular velocity-current plot, which is represented in Fig. 2. Based on the above estimation results, we verified the proposed modeling of the UAV motor for the steady-state and provided the basis for judging the normal driving conditions.

III. UAV Motor Faults Diagnosis

A. Faults Assumption and Injection

In this section, causes of the UAV motor failure are surveyed, and faults are selected to verify the performance of diagnosis. In addition, fault injection methods for experimental simulation are suggested. Common failures of electric motor have been caused by bearings, stators, and rotors, as well as other factor [28], [29]. This classification is not optimized to the UAV motor, but it can help to select the fault which may occur. Hence major and testable situations have to be chosen for each of these failure areas.

For general DC motor faults, damage to bearings are the most frequently encountered, which are classified into 6 categories according to ISO 15243:2004(E). A bearing can be susceptible to fatigue, wear, corrosion, electrical erosion, plastic deformation, and fracture or cracking. This study assumes that these damages commonly increase the dynamic friction because kinetic energy is lost to thermal or sound energy. The coil winding can be damaged by mechanical, electrical, thermal, or environmental stresses. The stator faults are categorized into short and open circuits and especially short-circuit faults are classified as detailed leakage point [39]. It is predicted that the problem is more likely to occur in the external than the internal coil of the stator structure due to physical impact or surface contact. Since phase wires of most UAV motors are exposed to the outside, phase faults are the main source of stator damage. If the phase wire is shorted to another, excessive current flows to the circuit and the entire motor system can immediately fail. For this reason, only the phase open fault is selected for diagnostic experiments for verification. If the UAV crashes into something in flight, the most vulnerable component is the fast spinning propeller. Furthermore, propeller has a larger radius, so blades can be broken or damaged even from a slight contact. In the UAV motor, the propeller is included in the rotor, so it is an important area for rotor faults. Most studies about the failure of UAV motors have focused on the propeller [15]-[19].

Previous studies on the classification of motor faults included the category 'others' which refers to eccentricity. But eccentricity can be included in 'bearing' or 'rotor' fault because it relates to the rotating assembly. As we mentioned above, the ESC is a component of the UAV motor that converts electrical energy into mechanical rotation. Therefore, it can cause malfunctions to the UAV motor by external disturbance or internal fatigue. Since our target is the UAV motor, we propose an 'ESC fault' as one of the subjects of the faults.

In literature about faults classifications of motor drives such as [40], and [41], transistor faults commonly occur. A stress on a transistor may become excessive because it carries the entire phase current. For a shorted transistor, a base drive should be immediately suppressed in order to prevent the phase current from continuously growing. So, we also exclude the transistor short fault for a similar reason as the stator fault. Since we use the sensorless motor which uses a back-EMF signal to drive, we add the fault of an abnormal back EMF signal.

In this study, the faults were classified into bearing faults (F1), stator faults (F2), rotor faults (F3), and ESC faults (F4). We selected in detail the faults of bearing friction increase (F1.1), phase open (F2.1), propeller damage (F3.1), transistor open (F4.1) and back EMF signal error (F4.2) respectively. To simulate these faults we used the following experimental methods. F1.1 and F3.1 were mechanically designed, which is represented in Fig. 3. In (a) of Fig. 3, a bar, which has a large coefficient of friction, was installed to a servo motor. The purpose of the bar is to push the side of the motor when F1.1 is injected. As shown (b) in Fig. 3, a partial broken propeller was used to simulate F3.1. The blades were trimmed to about 30% of their original length.

Fig. 4 is a circuit diagram of the fault injection module for F2.1, F4.1, and F4.2. To simulate F2.1, one of the phases connected from the ESC to the motor is cut off through the relay, and F4.1 is also applied to the transistor in the same way. When F4.2 is injected, the relay connects to ground the MCU pin of the back-EMF signal line.

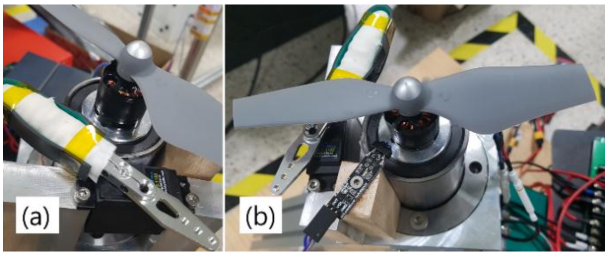

Figure 3. Experimental setting for fault injection of (a) F1.1 and (b) F3.1.

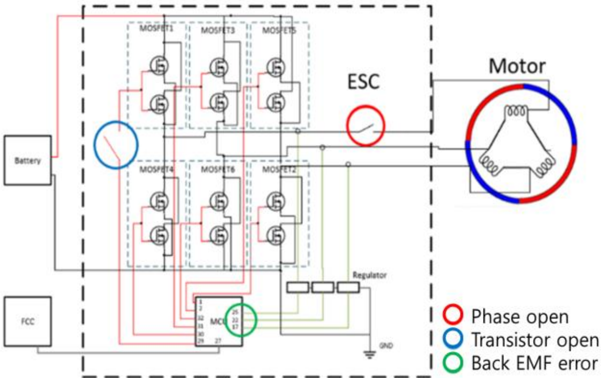

Figure 4. Schematic circuit diagram for F2.1, F4.1 and F4.2 of fault injection module

B. Faults Analysis and Diagnosis

The fault injection and diagnosis scheme are depicted in Fig. 5, and is designed to work as follows. The processors for fault injection and diagnosis are separated to two MCUs (STM32F407VE) for the possibility of independent diagnosis on a commercial vehicle. The PC transfers the fault injection commands to the MCU1 and receives the fault diagnosis result from MCU2. When F1 is injected, the servo motor is commanded to rotate by the

MCU1. For the F3, ordinary propeller is replaced with a broken propeller. In the case of the F2 and F4 injections, the MCU1 turns on the relay inside the fault module digitally. For simplicity and economy of the system, the voltage and current are measured on an entrance of the ESC, not on the phase. Since the infrared sensor generates the pulse by the motor rotation, the angular speed is calculated by frequency of the pulse. The measurements are read by the MCU2 and the diagnosis result is sent to the PC after the estimation of variables.

In order to diagnose faults, it was necessary to analyze not only the normal conditions but also characteristics of the fault. The data of selected faults were acquired for the steady-state of each input voltage. Angular speed and current plots for voltage are shown in Fig. 6 (a) and (b) respectively. The points on the graph represent averages at each point. Using the estimated model, the input voltage can estimate the steady state current and speed. Hence, we can confirm the possibility of prediction for the normal operation of the UAV motor.

If the friction increases in constant voltage, kinetic energy is lost. Therefore, from (2), the speed decreases and the current increases. In the case of F1.1, angular speed was slightly lower and the current was slightly higher than the estimations, so this result supports the theory. When the friction was larger than the test situation, F1.1 was more clearly distinguished from the normal operation because the difference between speed and current increased. The ESC of the sensorless motor determines the electrical angle using the back-EMF signal. A coil turning inside a magnetic field induces back-EMF which is included in the phase signal. If the phase is opened, the drive signal of the motor does not normally occur and current cannot flow in one phase.

In the case of F2.1, it was designed so that the motor starts to rotate and stop repeatedly, and the current constantly flows at about 3A. In most damaged propellers, thrust is reduced, so it is expected that k or C_p will decrease as described in (7). As a result, kinetic energy increases because friction by thrust decreases in contrast to F1.1. In the case of F3.1, angular speed was slightly higher and the current was slightly lower than the estimations, so this result can be explained theoretically. If a transistor is open, a connected phase with the transistor does not carry current even in the control sequence. However, by design the back-EMF is still measurable, unlike F2.1. The motor driving is disabled in one of the sequences and angular speed is expected to decrease. In the case of F4.1, both the angular speed and the current were smaller than the estimation, but the differences with normal condition were small at low speeds. In the case of F4.2, the results were similar to the motor operation of F2.1. Since the back-EMF signal is connected to the ground, the starting position of the motor cannot be figured out. But the phase and the currents flowing through the coil were healthy, so the current consumption was consistently higher than F2.1 at about 8A.

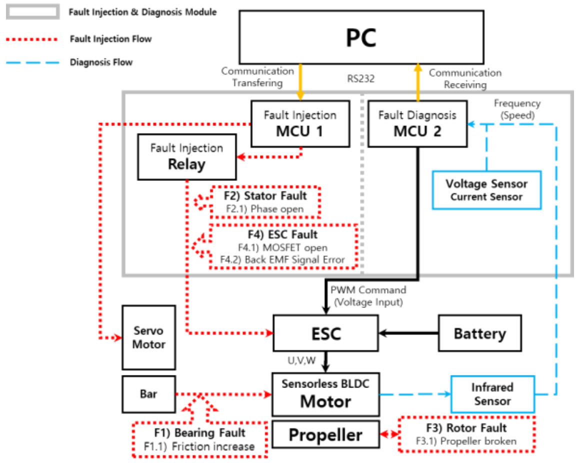

Figure 5. Flow chart of the motor fault injection and diagnosis

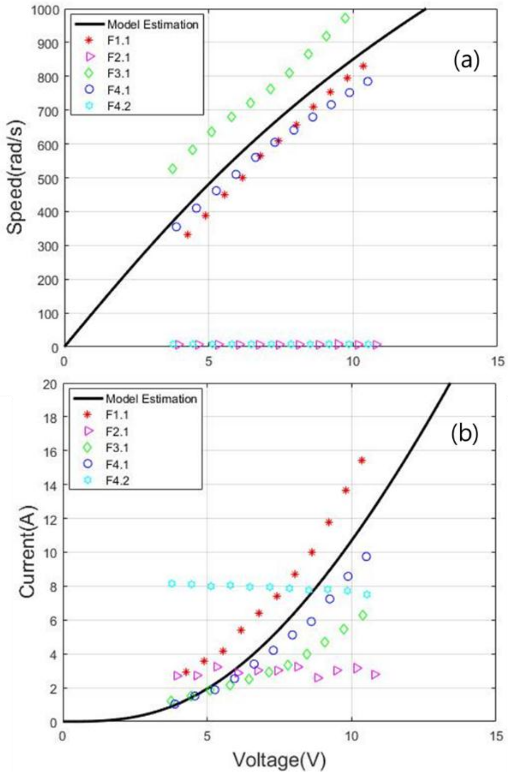

Figure 6. A comparison between estimated value and measured fault characteristics for the steady-state of the UAV motor: (a) input voltage vs. rotor speed and (b) input voltage vs. output current.

Each of the faults had a different consequence as shown, which were distinct to model estimation. First, we need to specify the interval of the model estimation to define the normal operation. Noises and errors of measurements are considered to ensure the reliability of the determination of fault detection. Since the noise of speed measurements are about ±10 rad/s, the interval of normal driving is defined as ±20 rad/s of the model estimation. As the input voltage increases, so does the current noise. Since the noise of the current varies from ± 0.15A minimum to ± 1.0A maximum, the determination interval of the normal operation is defined as ± 0.25~2.5A according to input size.

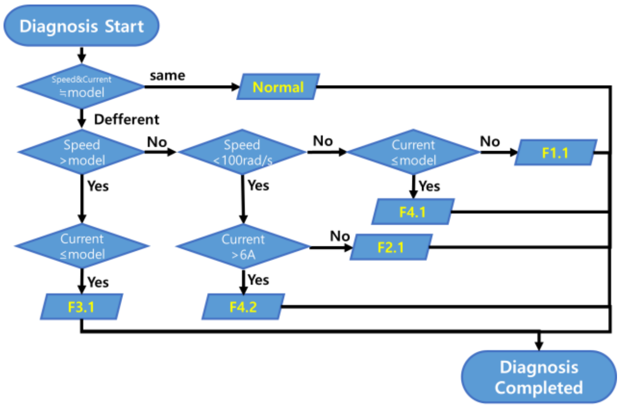

Figure 7. Flowchart of the proposed fault diagnosis algorithm.

Based on the fault analysis, we propose an algorithm that can diagnose the faults across the UAV motor for the steady-state condition. The F3.1 diagnosis algorithm includes the fact that the angular velocity is greater and the current is lower than the model estimation. F1.1 or F4.1 is diagnosed when the angular velocity is included or less than the estimated range. If the angular velocity is lower than 100 rad/s, F1.1 or F4.1 is diagnosed. In detail, F1.1 and F4.1 are diagnosed with whether the current is greater than the estimated, and F2.1 and F4.2 are diagnosed with whether the current is less than 6A. Fig. 7 shows the flowchart of the fault diagnosis algorithm. The proposed algorithm is designed to be as simple as possible to diagnose the selected faults.

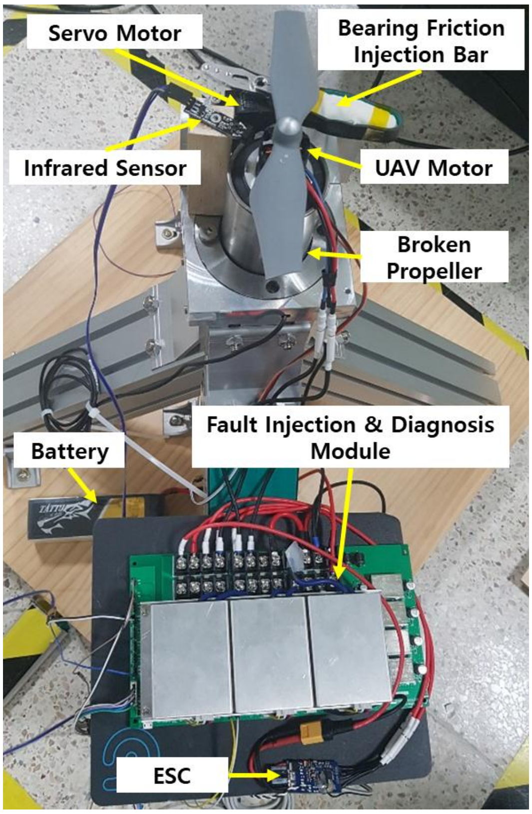

Figure 8. Experimental setup of the UAV motor testbed for fault injection and diagnosis.

IV. Experimental Verification

A. Fault Diagnosis Experiments on the Testbed

The configuration of the experimental setup to inject faults and to verify diagnostic performance is shown in Fig. 8. UAV motors were installed at a height at least three times the radius of the propeller to minimize ground effects [42], [43]. Since the height is 520mm, the ratio of the radius to the height was about 4.3:1. The infrared sensor was placed facing the motor to measure the pulse output by the spin of the rotor. All the sensors were read to MCU2 in 200 Hz, but the sampling rate of the data was 40Hz. A five moving average filter is applied to current measurements and it reduces noise in the steady-state. The lithium polymer battery which can be applied in the flight model is used. The ESC and the UAV motor were connected to the fault injection & diagnosis module. For the F1.1, the servo motor was fixed under the propeller and rotated the bar which was covered with rubber. The broken propeller was used for F3.1 and replaced in other experiments.

The experiments were planned to diagnose all the selected faults across the operating speed range. Verification was required at various input voltages, because the model of the UAV motor was nonlinear. Therefore, the experiments were divided into five cases in 4.2V, 5.8V, 7.6V, 9.2V and 11V respectively. Input voltage was held constant and the fault was injected at a certain time to confirm the diagnosis result. Fig. 9 to 13 shows the experimental results during ten seconds before and after the selected faults injection, except Fig. 11 which the UAV motor was started at five seconds. Experimental results with an increasing input voltage are presented in each graph from left to right in the figures. The black dashed line indicates the input values such as the speed or current estimation and the fault injection command. The blue line is the real time measurements and the red line is the fault diagnosis value.

Fig. 9 shows that fault diagnosis converges to F1.1 as speed decreases and current increases for the steady-state after F1.1 injection. The speed converged after about 0.5 seconds from the F1.1 injection, but the maximum diagnosis time is about 1.1 seconds due to the time of current convergence. In Cases 2 and 3, F4.1 was diagnosed for a short time during the transient state, since the current is within the normal range. Fig. 10 shows that fault diagnosis converges to F2.1 within 0.8 seconds. Speed decreased to almost zero while the current was maintained at 2 to 4 A for the steady-state after the F2.1 injection. The speed converged in 0.3 seconds, which is faster than the diagnosis, and F4.1 was diagnosed until the speed was less than 100 rad/s for the transient period. For Cases 4 and 5 with high currents, F4.2 is diagnosed until the current is below 6A. Since breaking a propeller in the middle of the UAV motor spinning is dangerous, the F3.1 experiment was carried out using the pre-broken propeller as indicated in Fig. 8. Fig. 11 plots the data from these experiments. The F2.1 was diagnosed during speeds measuring lower than 100 rad/s. Since the current flow was less than the estimation and the speed measurement passed through the estimated range, the diagnosis shifts to F4.1 for a moment. F3.1 was diagnosed within 0.35 seconds, according to the results in which the speed was above the normal range. Fig. 12 shows that the diagnosis corresponds with the fault injection even in transient-state. The diagnostic time of Case1 was the longest at 0.43 seconds, because the estimation error was the maximum among the cases. When F4.2 was injected, angular speed dropped to under 100 rad/s and current flows remained at about 7 to 8A. It is shown in all the cases in Fig. 13. F2.1 was diagnosed during the current rising from 6A in cases 1 and 2 whereas F1.1 was diagnosed in the other cases until below 100 rad/s for a short time. The F4.2 diagnosis experiment of Case1 took the longest time of 0.9 seconds among the all cases.

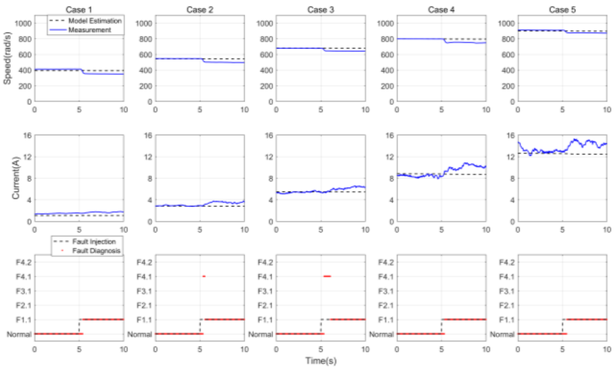

Figure 9. F1.1 injection and diagnosis experiments on the testbed.

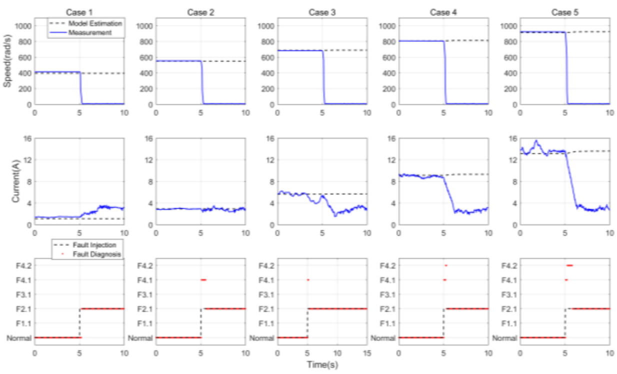

Figure 10. F2.1 injection and diagnosis experiments on the testbed.

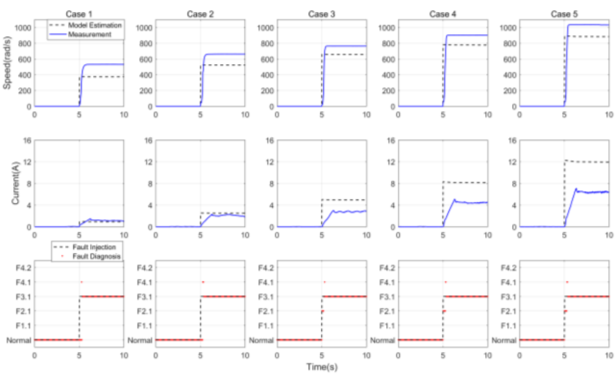

Figure 11. F3.1 injection and diagnosis experiments on the testbed.

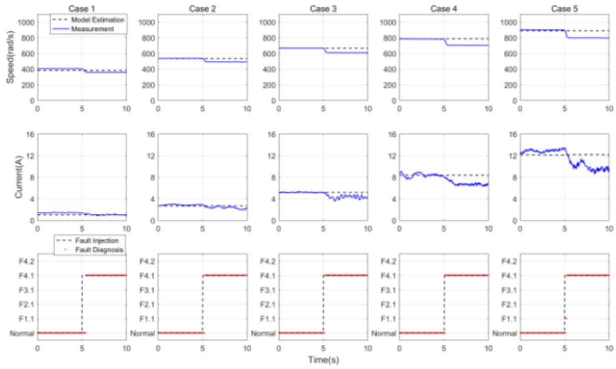

Figure 12. F4.1 injection and diagnosis experiments on the testbed.

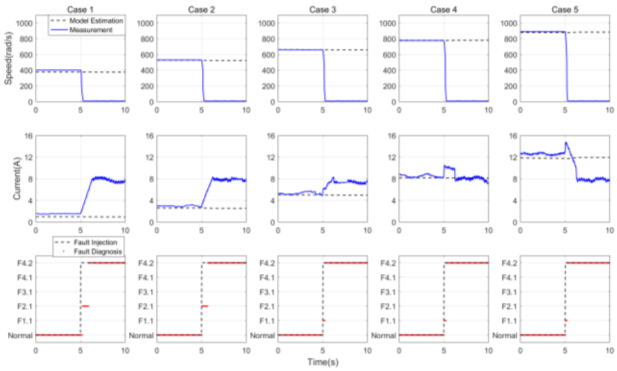

Figure 13. F4.2 injection and diagnosis experiments on the testbed.

Thrust did not occur for the F2.1 and F4.2, when the UAV motor almost stopped. If these two faults occur, the diagnosis speed may be important because the drone has to apply a fault tolerant control. Thus, using diagnosis in the transient state is possible regardless of F2.1 or F4.2. If this method is applied, then a failure of the UAV motor is determined within 0.25 seconds. Except for the above situations, the diagnosis only in the steady-state is advisable for practical applications.

B. Flight Test Results for Application

When the UAV motor is fixed on the floor and the input voltage is stable, experiments cannot prove that the proposed technique has effected during flight. Therefore, additional flight tests for fault diagnosis are necessary to validate drone application. Fig. 14 shows the experimental scene where a hexacopter hovers with a weight of 5 kg and a diameter of 1m. F1.1 and F3.1 are difficult to implement on the hexacopter, so these are excluded from the flight test, while F2.1, F4.1, and F4.2 are selected for their ability to be electrically injected. While the drone controlled the attitude for stability, the selected faults were injected into the UAV motor, and we observed the angular speed, current, and fault diagnosis results until the steady-state.

In Fig. 15, 16, and 17, plots of the flight tests are numbered in order of stability of input voltage. The UAV motor stopped and the current was maintained at about 2.26A on average after the F2.1 fault was injected. As shown in Fig. 15, all of the F2.1 test results reveal that diagnosis data is obtained same to inject faults. For the F4.2 injection test results, the UAV motor stopped in the same way as the F2.1 tests, and the current flowed at 7.73A on average. Since the measured current decreased below 6A, Fig. 16 shows that the diagnosis error rose to 2.44% in the F4.2 test. This is because the diagnostic algorithm for the testbed was applied to the flight tests without modification. Thus the algorithm needs to be optimized for the flight model. F4.1 injection tests showed that the diagnostic performance was affected by the stability of the control, which is represented in Fig. 17. The timeliness and accuracy of the fault diagnosis of test no.1 to 3 are analyzed as 0.1s-98.49%, 0.2s-93.70% and 1.4s-71.85%, respectively. Since the input voltage changes constantly, the transient state cannot be easily defined. For that reason, diagnostic accuracy was calculated at all ranges after the fault injection. Hence the results do not reflect the accuracy of the proposed technique, but it does help to check the variation of the diagnostic performance according to stability of the input. Meanwhile, the proposed model estimated the normal operation to an accuracy of 99.11% even with fluctuating input.

In order to apply the fault diagnosis algorithm to the flight model, the conditions regarding the steady-state have to be defined additionally. Furthermore, the diagnostic technique for various environments of drone operation can be advanced to model-based neural networks.

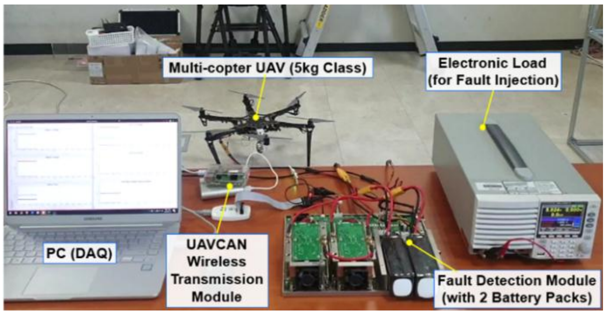

Figure 14. Flight Test setup of the UAV motor for fault injection and diagnosis.

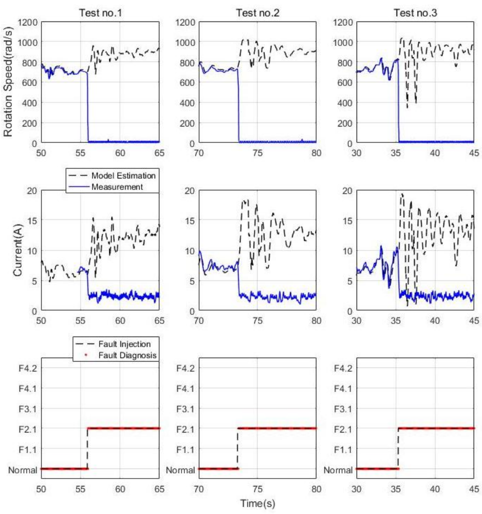

Figure 15. F2.1 injection and diagnosis experiments in flight.

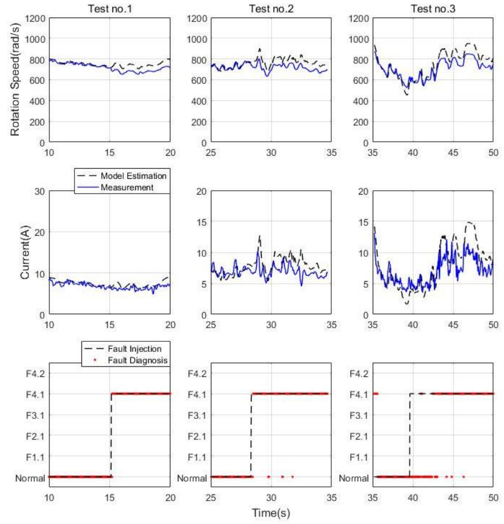

Figure 16. F4.2 injection and diagnosis experiments in flight.

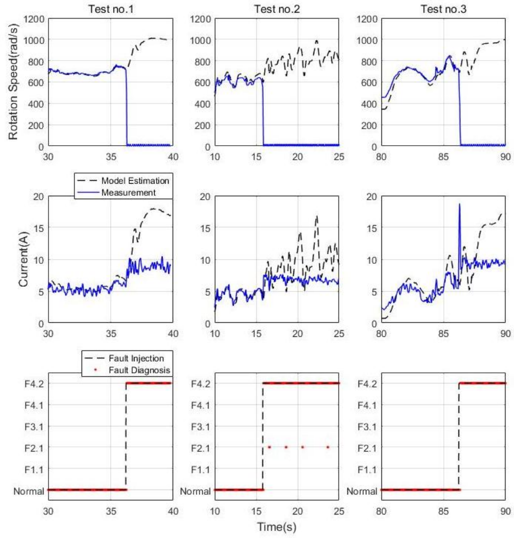

Figure 17. F4.1 injection and diagnosis experiments in flight.

C. Discussion

The proposed model properly estimated the normal operation of the UAV motor for all of the tests on the testbed as well as in flight. Even though unstable performance of diagnosis in transient state, the results in the steady-state are valuable in this study. Nevertheless, simulated faults were diagnosed well in flight tests when the fluctuation of the input voltage of the UAV motor was not too steep. In general, if the attitude of the drone is more stable, convergence speed with the steady-state will be fast and the UAV motor input will be more stable. Also, if current sensor performance is improved, measurement noise will be reduced and measurement will be more accurate. These two methods for a high-quality UAV system will help to advance the proposed technique.

Although not included in this paper, overcurrent may occur instantaneously in case of short circuit failure. In this case, it is necessary to measure the current in transient state and shut off the input immediately for safety.

V. CONCLUSION

This paper proposed a nonlinear steady-state model of the UAV motor using previous works and theoretical relations. Compared to current and velocity data, the accuracy of the estimated model is 99%. Dynamic friction increase, phase open, propeller broken, transistor open and back EMF signal error are experimented by manually injection. The simple diagnosis algorithm are designed by analyzing the each steady-state characteristics from fault injection experiments. Testbed experimental results showed that all the faults are successfully diagnosed for the steady-state. Flight tests are conducted for hexacopter during hovering state and diagnostic accuracy in stable condition was about 98%. These results validate that the diagnosis performance can be applied to commercial drones. Although most studies about fault diagnosis have dealt with just one fault type such as stator or rotor, the proposed technique has the advantage of diagnosing various faults by monitoring basic variables of the motor. For practical application, repetitive testing is necessary to verify the reliability, and complicated and advanced diagnosis algorithms have to be further studied depending on the environment. This diagnostic technique can help with the decision making of the repair or replacement before more serious or complete failures of the UAV motor.

CONFLICT OF INTEREST

The authors declare no conflict of interest

AUTHOR CONTRIBUTIONS

Jun-yong Lee proposed the faults diagnosis idea and wrote the paper; Won-tak Lee conducted the experiments; Sang-ho Ko and Hwa-suk Oh analyzed the data; all authors had approved the final version.

ACKNOWLEDGMENT

This research was supported by Unmanned Vehicles Advanced Core Technology Research and Development Program through the National Research Foundation of Korea(NRF), Unmanned Vehicle Advanced Research Center(UVARC) funded by the Ministry of Science, ICT and Future Planning, the Republic of Korea (2016M1B3A1A03937725)..

REFERENCES

[1] B. Custers, *The Future of Drone Use: Opportunities and Threats from Ethical and Legal Perspectives*, Springer, 2016, vol. 27.

[2] D. Chabot, “Trends in drone research and applications as the journal of unmanned vehicle systems turns five,” *Journal of Unmanned Vehicle Systems*, vol. 6, no. 1, pp.: vi–xv, 2018.

[3] M. M. Nasir and Q. Shi-Yin, “Notice of violation of IEEE publication principles: Investigation of human factors in UAV accidents based on analysis of statistical data,” in *Proc. 2011 First International Conference on Instrumentation, Measurement, Computer, Communication and Control*, Beijing, 2011, pp. 1011-1015.

[4] M. Oncu and S. Yildiz, “An analysis of human causal factors in unmanned aerial vehicle (uav) accidents,” Naval Postgraduate School, Monterey, California, 2014.

[5] K. P. Valavanis and G. J. Vachtsevanos, *Handbook of Unmanned Aerial Vehicles*, Springer Netherlands, 2015.

[6] Q. Quan, *Introduction to Multicopter Design and Control*, Singapore: Springer, 2017.

[7] Z. Cen, H. Noura, T. B. Susilo, and Y. Al Younes, “Robust fault diagnosis for quadrotor uavs using adaptive thau observer,” *Journal of Intelligent & Robotic Systems*, vol. 73, no. 1-4, pp. 573–588, 2014.

[8] M. Saied, H. Shraim, C. Francis, I. Fantoni, and B. Lussier, “Actuator fault diagnosis in an octorotor UAV using sliding modes technique: Theory and experimentation,” in *Proc. Eur. Control Conf. (ECC)*, July 2015, pp. 1639–1644.

[9] W. Han, Z. Wang, and Y. Shen, “Fault estimation for a quadrotor unmanned aerial vehicle by integrating the parity space approach with recursive least squares,” *Proc. Inst. Mech. Eng. Part G: J. Aerosp. Eng.1*, 2017.

[10] Y. Zhong, Y. Zhang, W. Zhang, J. Zuo, and H. Zhan, “Robust actuator fault detection and diagnosis for a quadrotor UAV with external disturbances,” *IEEE Access*, vol. 6, pp. 48169–48180, 2018

[11] A. Freddi, S. Longhi, A. Monteriu, and M. Prist. “Actuator fault detection and isolation system for an hexacopter,” *10th Intern. Conf. on Mechatronic and Embedded Systems and Applications*, Senigallia, Italy, pp. 1-6, 2014.

[12] M. Saied et al., “Fault diagnosis and fault-tolerant control strategy for rotor failure in an Octorotor,” in *Proc. International Conference on Robotics and Automation*, Washington, May 2015.

[13] M. Saied, B. Lussier, I. Fantoni, H. Shraim, and C. Francis, “Fault diagnosis and fault-tolerant control of an Octorotor UAV using motors speeds measurements,” *IFAC PapersOnline 50-1(2017) 5263-5268*.

[14] Y. A. Younes, H. Noura, A. Rabhi, and A. E. Hajjaji, "Actuator fault-diagnosis and fault-tolerant-control using intelligent-output-estimator applied on quadrotor UAV," *2019 International Conference on Unmanned Aircraft Systems (ICUAS)*, Atlanta, GA, USA, 2019, pp. 413-420

[15] F. Pourpanah, B. Zhang, R. Ma and Q. Hao, "Anomaly detection and condition monitoring of UAV motors and propellers," *2018 IEEE SENSORS*, New Delhi, 2018, pp. 1-4.

[16] A. Bondyra, P. Gasior, S. Gardecki and A. Kasiński, "Fault diagnosis and condition monitoring of UAV rotor using signal processing," *2017 Signal Processing: Algorithms, Architectures, Arrangements, and Applications (SPA)*, Poznan, 2017, pp. 233-238.

[17] A. Benini, F. Ferracuti, A. Monteriù, and S. Radensleben, "Fault detection of a VTOL UAV using acceleration measurements," in *Proc. 2019 18th European Control Conference (ECC)*, Naples, Italy, 2019, pp. 3990-3995.

[18] J. Fu, C. Sun, Z. Yu and L. Liu, "A hybrid CNN-LSTM model based actuator fault diagnosis for six-rotor UAVs," in *Proc. 2019 Chinese Control And Decision Conference (CCDC)*, Nanchang, China, 2019, pp. 410-414.

[19] G. Iannace, G. Ciaburro and A. Trematerra, “Fault diagnosis for UAV blades using artificial neural network," *Robotics*, 2019, 8, 59.

[20] M. L. Sin, W. L. Soong, and N. Ertugrul, “Induction machine on-line condition monitoring and fault diagnosis—A survey,” in *Proc. Australian Universities Power Eng. Conf.*, Chrischurch, New Zealand, 2003.

[21] A. J. Bazurto, E. C. Quispe and R. C. Mendoza, "Causes and failures classification of industrial electric motor," in *Proc. 2016 IEEE ANDESCON*, Arequipa, 2016, pp. 1-4.

[22] O. Moseler and R. Isermann, "Application of model-based fault detection to a brushless DC motor," *IEEE Transactions on Industrial Electronics*, vol. 47, no. 5, pp. 1015-1020, Oct. 2000.

[23] M. A. Awadallah and M. M. Morcos, "ANFIS-based diagnosis and location of stator interturn faults in PM brushless DC motors," *IEEE Transactions on Energy Conversion*, vol. 19, no. 4, pp. 795-796, Dec. 2004.

[24] M. A. Awadallah, M. M. Morcos, S. Gopalakrishnan, and T. W. Nehl, "A neuro-fuzzy approach to automatic diagnosis and location of stator inter-turn faults in CSI-fed PM brushless DC motors," *IEEE Transactions on Energy Conversion*, vol. 20, no. 2, pp. 253-259, June 2005.

[25] M. A. Awadallah and M. M. Morcos, "Automatic diagnosis and location of open-switch fault in brushless DC motor drives using wavelets and neuro-fuzzy systems," *IEEE Transactions on Energy Conversion*, vol. 21, no. 1, pp. 104-111, March 2006.

[26] S. Rajagopalan, J. M. Aller, J. A. Restrepo, T. G. Habetler and R. G. Harley, "Detection of rotor faults in brushless DC motors operating under nonstationary conditions," *IEEE Transactions on Industry Applications*, vol. 42, no. 6, pp. 1464-1477, Nov.-dec. 2006.
[27] B. Park, K. Lee, R. Kim, T. Kim, J. Ryu and D. Hyun, "Simple fault diagnosis based on operating characteristic of brushless direct-current motor drives," *IEEE Transactions on Industrial Electronics*, vol. 58, no. 5, pp. 1586-1593, May 2011.
[28] A. Tashakori and M. Ektesabi, "Fault diagnosis of in-wheel BLDC motor drive for electric vehicle application," in *Proc. 2013 IEEE Intelligent Vehicles Symposium (IV)*, Gold Coast, QLD, 2013, pp. 925-930.
[29] J. Fang, W. Li, H. Li and X. Xu, "Online inverter fault diagnosis of buck-converter BLDC motor combinations," in *IEEE Transactions on Power Electronics*, vol. 30, no. 5, pp. 2674-2688, May 2015.
[30] P. C. Krause, *Analysis of Electric Machinery and Drive Systems*, Piscataway, NJ: IEEE Press, 2002.
[31] R. Krishnan, *Switched Reluctance Motor Drives—Modeling, Simulation, Analysis, Design, and Applications*, Boca Raton, FL: CRC Press, 2001.
[32] J. Pan, N. Farag, T. Lin, et al. "propeller induced structural vibration through the thrust bearing," *Innovation in Acoustics and Vibration Annual Conference of the Australian Acoustics Society*, 2002, Adelaide, Australia, November 2002:390-399.
[33] M. Ryll, H. H. Bülthoff, and P. R. Giordano, "A novel overactuated quadrotor unmanned aerial vehicle: Modeling, control, and experimental validation," *IEEE Transactions on Control Systems Technology*, vol. 23, no. 2, pp. 540-556, March 2015.
[34] K. Li, S. K. Phang, B. M. Chen, and T. H. Lee, "Platform design and mathematical modeling of an ultralight quadrotor micro aerial vehicle," in *Proc. the 2013 International Conference on Unmanned Aircraft Systems*, Atlanta, USA, pp. 1066-1075, May 2013.
[35] L. Wu, Y. Ke and B. M. Chen, "Systematic modeling of rotor dynamics for small unmanned aerial vehicles," in *Proc. International Micro Air Vechicle Competition and Conference*, Beijing, 2016, p. 284-290.
[36] C. Zhao, X. Yu, Q. Huang, S. Ge, and X. Gao, "Analysis on the load characteristics and coefficient of friction of angular contact ball bearing at high speed," *Tribol. Int.*, vol. 87, pp. 50-56, 2015.
[37] M. R. D. Balan, L. Houpert, A. Tufescu, and D. N. Olaru, "Rolling friction torque in ball-race contacts operating in mixed lubrication conditions," *Lubricants*, vol. 3, no. 2, pp. 222-243, 2015.
[38] D. Muzar and E. Lanteigne, "Experimental characterization of brushless DC motors and propellers for flight application," in *Proc.* of *the Canadian Society for Mechanical Engineering International Congress 2016*, June 2016.
[39] S. Karmakar, S. Chattopadhyay, M. Mitra, and S. Sengupta, *Induction Motor Fault Diagnosis Diagnosis: Approach through Current Signature Analysis*, Springer, 2016.
[40] P. Kadaněk, *A Brief Survey of AC Drive Fault Diagnosis & Detection*, Prague, December 1998
[41] D. Kastha and B. K. Bose, "Investigation of fault modes of voltage-fed inverter system for induction motor drive," *IEEE Transactions on Industry Applications*, vol. 30, no. 4, pp. 1028-1038, July-Aug. 1994.
[42] P. Sanchez-Cuevas, G. Heredia, and A. Ollero, "Characterization of the aerodynamic ground effect and its influence in multirotor control," *Int. J. Aerosp. Eng.*, vol. 2017, Art. no. 1823056.
[43] D. D. C. Bernard, M. Giurato, F. Riccardi, et al., "Ground effect analysis for a quadrotor platform," *Advances in Aerospace Guidance, Navigation and Control*. Springer, 2018, pp. 351–367.

Jun-yong Lee was born in Incheon, Republic of Korea in 1988. He received the B.S. and M.S. degrees in aerospace engineering from the Korea Aerospace University, Goyang, in 2014 and 2016, respectively, where he is currently working toward the Ph.D. degree. From 2018 to 2019, he was with the Revoluti co., Korea, as a Researcher. His research interests include attitude control of satellite, space environment, actuators, modeling and control of electrical motor systems, and CMG applications.

Won-tak Lee was born in Seoul, South Korea in 1993. He received the B.S. and M.S. degrees in Mechanical Engineering from the Korea Aerospace University, Goyang City, in 2020.02. Now, he is working at LGC(Research Park in Daejeon, LG Chemistry) as a researcher of Lithium-ion Battery department. Development of new algorithms or logics detecting failures of ESS(Energy Storage System) is his main tasks. Offering preventative measures against Fire Issues arouses his interests.

Sang-ho Ko is a professor at the School of Aerospace and Mechanical Engineering, Korea Aerospace University, South Korea. He received his Ph.D. degree from the Department of Mechanical and Aerospace Engineering of the University of California, San Diego (UCSD) in 2005. From 2005 to 2006, he was a post-doctoral scholar in UCSD to research system identification techniques. From March 2006 to February 2008 he was a research fellow in the Department of Electrical and Electronic Engineering of the University of Melbourne, Australia, where he worked on finite sample quality assessment of system identification. From 1992 to 1999, he was with Samsung Aerospace Industries, Ltd., Gyungnam, Korea, where he was a research and development engineer for digital flight control systems. His research interests include: state estimation and control, system identification, flight control, propulsion system control.

Hwa-suk Oh received his Ph.D. degree in Aerospace Engineering from Texas A&M University in 1992. After spending several years in ETRI in Korea, he is currently a professor of the School of Aerospace and Mechanical Engineering at Korea Aerospace University. Since His research interests include satellite attitude control and determination. Recent researches are concentrated into developing attitude hardware such as reaction wheel, CMG, MEMS IMU, etc.